SANDIA REPORT
SAND2024-09214
Printed July 2024

Sandia National Laboratories

Effect of Hot Isostatic Pressing on the Microstructure and Mechanical Properties of Additively Manufactured Ti alloys

Josh Sugar, Bonnie Antoun, Ryan Nishimoto, Javier Cebrian, Meghan Rogers, Jeff Chames, and Tyler Lebrun

Prepared by
Sandia National Laboratories
Albuquerque, New Mexico
87185 and Livermore,
California 94550

Issued by Sandia National Laboratories, operated for the United States Department of Energy by National Technology & Engineering Solutions of Sandia, LLC.

Available to DOE and DOE contractors from
U.S. Department of Energy
Office of Scientific and Technical Information
P.O. Box 62
Oak Ridge, TN 37831

Telephone: (865) 576-8401
Facsimile: (865) 576-5728
E-Mail: reports@osti.gov
Online ordering: http://www.osti.gov/scitech

Available to the public from
U.S. Department of Commerce
National Technical Information Service
5301 Shawnee Rd
Alexandria, VA 22312

Telephone: (800) 553-6847
Facsimile: (703) 605-6900
E-Mail: orders@ntis.gov
Online order: https://classic.ntis.gov/help/order-methods/

ABSTRACT

A previous SAND report, SAND2020-11353 described the basic metallurgical and surface roughness properties of additively manufactured Ti-64 material made using a powder bed fusion process. As part of that work, material was post-processed using a hot isostatic press (HIP) to densify and heat treat the material. This report is meant as an addendum to the original report and to provide specific data on material processed with HIP. The main focus of this report is to show the effects of HIP on the microstructure and mechanical properties of AM Ti-64 and Ti-5553.

CONTENTS

LIST OF FIGURES

LIST OF TABLES

This page left blank

ACRONYMS AND TERMS

Acronym/Term	Definition
AM	additive manufacturing
Ti-64	Ti-6Al-4V alloy (in wt. %)
Ti-5553	Ti-5Al-5Mo-5V-3Cr (in wt. %)
HIP	hot isostatic press
PBF	powder bed fusion
EDS	energy dispersive spectroscopy
EBSD	electron back-scattered diffraction
SEM	scanning electron microscopy
SE	secondary electron
BSE	back-scattered electron
KCP	Kansas City Plant (the same as KCNSC, Kansas City National Security Campus)
Hcp	Hexagonal close packed
Bcc	Body-centered cubic
α	Alpha-phase hcp titanium
β	Beta-phase bcc titanium
DED	directed-energy deposition
BC	Band Contrast
IPF(X,Y,Z)	inverse pole figure parallel to X, Y, or Z
GND	geometrically necessary dislocations
ECD	Equivalent circle diameter

1. INTRODUCTION

A previous report investigated a wide variety of AM-processed Ti alloys.[1] That study is the result of several years of work. There were some aspects of that work that was not complete in 2020 and did not get reported in that document. Because of personnel changes at Sandia, this work had to be handed off to other members of the workforce who could bring the final aspects of the work to closure and report on it. The purpose of this report is to bring closure to the unfinished aspects of the previous work. The content of this report will focus on the effects of HIP on mechanical processing and microstructure in the AM Ti-64 and Ti-5553 alloys.

Ti alloys generally consist of an alpha hcp phase and/or a beta bcc phase. Ti-64 is one of the most widely used Ti-alloys, and is considered an α-β alloy because it generally consists of a mixture of the α and β phases. The strength of Ti-64 can be tuned through solution treating and aging. Depending on the solution treatment temperature, cooling rate, the section size, and the alloy composition, a heat treatment in the α-β field followed by a quench will result in the β phase being retained, partly, or fully transformed to the α phase [2, 3].

Ti-5553 is another heat treatable alloy that has additional beta stabilizers in it that delay the α precipitation onset and preserve the beta phase. As a result, it has improved strength-toughness combinations in thicker gage sections [4]. Ti-5553 is often referred to as a "near-β" titanium alloy, and achieves strengthening through precipitation of the alpha phase. Where cooling of Ti-64 often results in most of the beta phase transforming to alpha, in Ti-5553 the additional beta stabilizers shift the composition so that when cooled below the β transus, α precipitates in the two phase field as the minor phase.

Since both of these alloys are fabricated using AM PBF technology, they are rapidly cooled from the melt. This leads to solidification microstructures in the as-built condition, that then get modified during HIP. This report will show the evolution of the microstructure and the mechanical properties as a result of HIP on AM Ti-64 and Ti-5553 alloys.

2. MATERIALS AND METHODS

2.1. Materials Fabrication

The AM material used in this study is the same as what was used in [1]. Both the Ti-64 and Ti-5553 alloys were fabricated using a laser PBF process. Briefly, in laser PBF, a bed of powder is selectively melted with a laser in a pattern that consistent with a single slice of the final part geometry. A stage then lowers one layer thickness down, and then a new layer of unmelted powder is spread onto the bed. The laser then selectively melts the next layer in the structure, and this process repeats over and over until the final part geometry is reached. All parts tested in this report were fabricated at KCP.

2.2. Mechanical Testing

The mechanical tests were performed at SNL CA in the Mechanics of Materials Laboratory on a Hi Rate MTS servohydraulic test frame. The test frame load cell and actuator (displacement) are calibrated yearly according to Sandia's PSL standards. The tensile specimens (shown in Figure X) had a total length of 1.70 in (43.18 mm), with a straight gage section of 0.593 in (15.06 mm) and gage diameter of 0.100 in (2.54 mm). The exact gage diameter was measured on each specimen using a Keyence IM measurement microscope, this measurement was used to calculate stress from the measured load.

The tensile tests were controlled using MTS Flextest programmable software. All tests were conducted in actuator displacement control at a rate of 0.0007 in/s (0.01778 mm/s) to produce a strain rate of approximately 0.001/s. A 0.5 in (12.7 mm) gage length contacting extensometer (MTS Model 632.12 B-20, Serial Number 455) was attached to each specimen, centered within the 0.592 in gage straight gage section. Data signals (time, actuator stroke/displacement, load, extensometer reading) were collected via the MTS Elite software at a rate of 1000 Hz. The extensometer remained attached through the duration of the test to failure to accurately measure actual specimen strain in the gage section. The reported elongation to failure strains were determined from this direct contact method on each specimen. Reduction in area measurements were determined by measuring each failure surface on a Keyence VHX microscope, taking the average of the two broken failed surfaces for each specimen, and comparing to the original gage area.

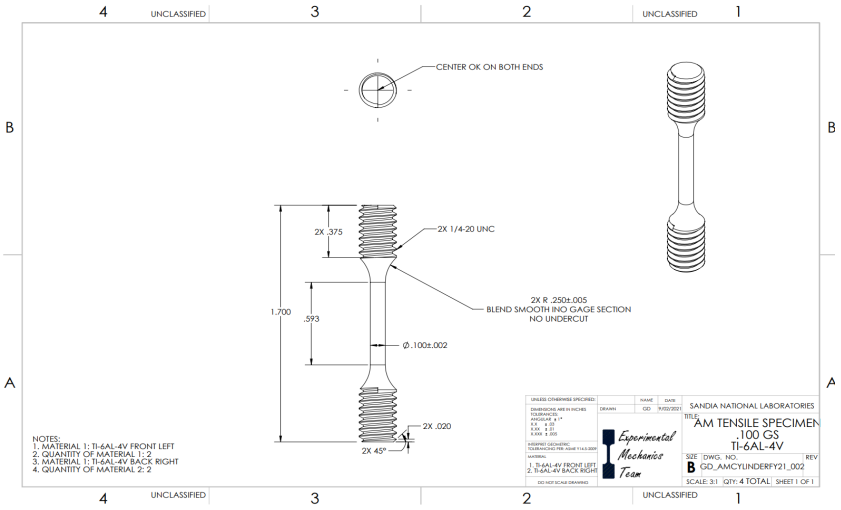

Figure 1: Tensile Specimen Geometry

2.3. Microstructural Characterization

Microstructural characterization was performed using a variety of SEMs at the CA microscopy lab. Samples were cut and metallographically mounted and polished prior to investigation. A JEOL 7600F with a Oxford Nordlys Max 2 EBSD and Extreme 80 EDS detector, or a ThermoFisher Apreo LoVac with a Bruker Quantax 60 EDS and a e- flash FS EBSD were used for data acquisition. A Keyence VK-X laser confocal profilometer was used to measure surface roughness.

2.4. HIP Processing

HIP processing of alloys was performed at Bodycote. The Ti-64 alloys was processed at Bodycote in Camas, WA. The Ti-5553 alloy was processed at Bodycote in Princeton, KY. The temperature and pressure schedule for the Ti-64 alloy is shown in Figure 2. According to a pseudobinary phase diagram for Ti-64 in [5], the heat treatment temperature of 1650°F is low enough as to keep the TI-64 in the alpha region of the phase diagram. It would be expected that only coarsening occurs during this treatment. Phase content of the alloy would not be expected to change.

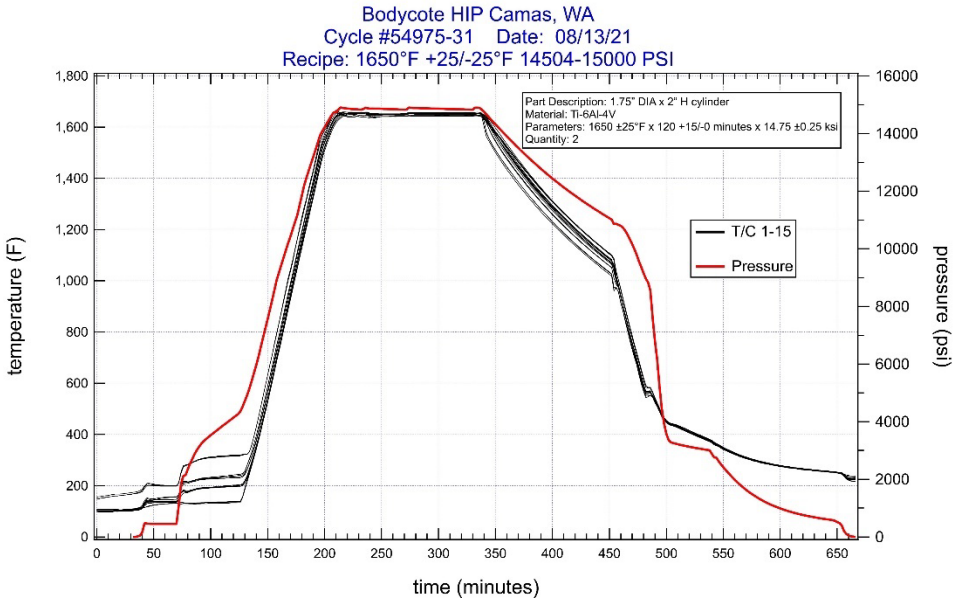

Figure 2: Time/Temperature/Pressure schedule for HIP processing of AM Ti-64.

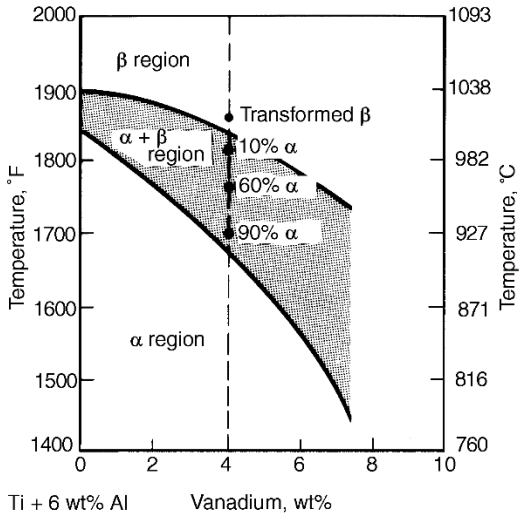

Figure 3: Pseudo Binary Phase Diagram for Ti-64 from [5]

The HIP processing parameters for Ti-5553 is shown in Figure 4. For Ti-5553, the hold temperature of 1499°F is below the alpha → beta solidus in the pseudo binary phase diagram (Figure 5 [4]). Therefore, we expect that the Ti-5553 alloy should develop some alpha phase during the HIP processing.

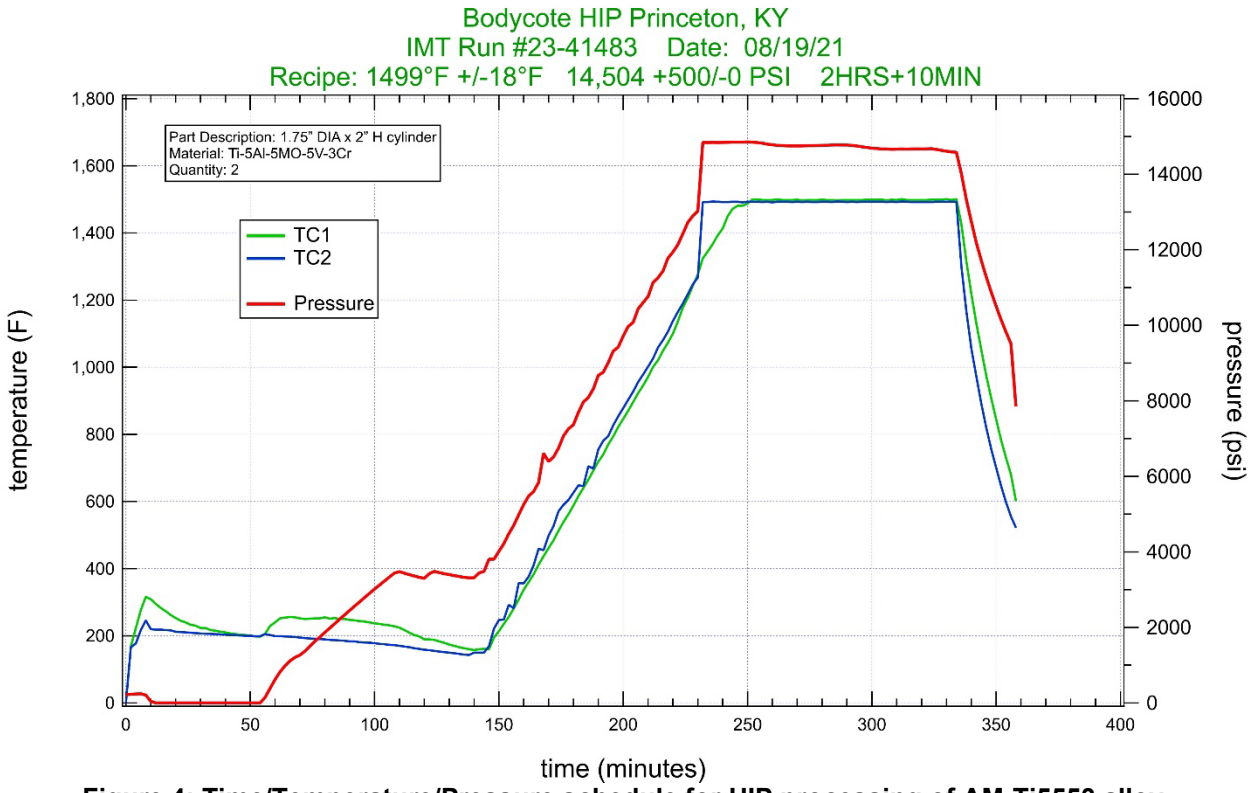

Figure 4: Time/Temperature/Pressure schedule for HIP processing of AM-Ti5553 alloy.

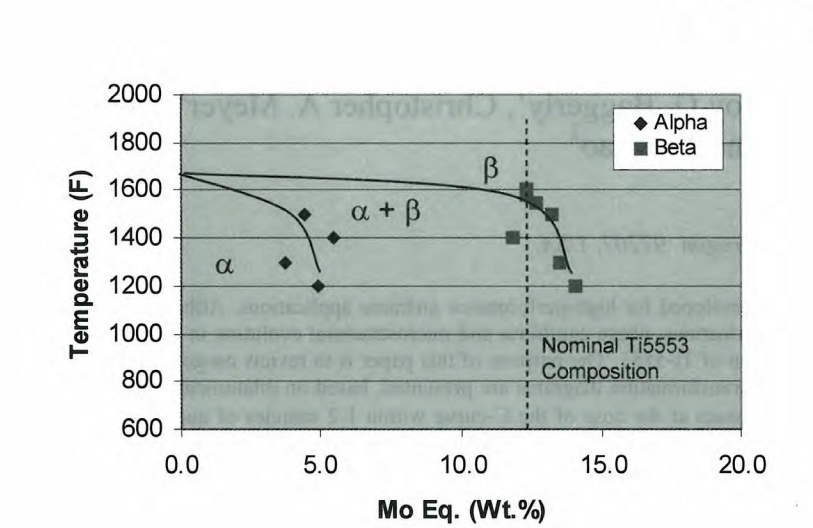

Figure 5: Approximate pseudobinary phase diagram for Ti-5553 from [4].

3. RESULTS AND DISCUSSION

3.1. Mechanical Tests

The effect of HIP processing on AM Ti-64 is shown in Figure 6. The stress-strain plots show that there is a lowering of the yield stress and an increase in elongation after the HIP processing. During HIP, it is expected that some flaws and defects and internal porosity should shrink in size. Since these flaws could be the critical flaws for crack nucleation during fracture, shrinking or eliminating them increases the ductility and elongation. It has been shown in DED stainless steel that large lack of fusion defects can degrade tensile and fatigue behavior [6]. It is expected that if defects did exist in this material after fabrication, the HIP process should help decrease the number and size of those defects. In addition, annealing at high temperatures during HIP could be reducing the number of microstructural defects that cause the high yield strength (e.g. thermal strain induced dislocations), and results in a lower yield strength after HIP. This behavior is typically expected during the recrystallization process, for example.

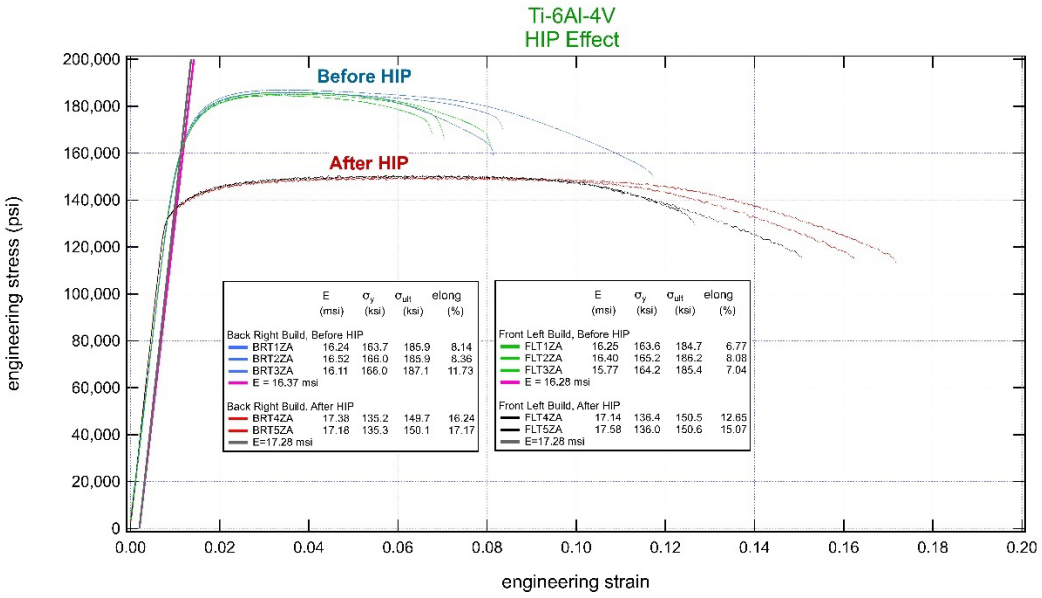

Figure 6: Effect of HIP processing on AM Ti-64.

A summary of the properties before and after HIP processing are shown in Table 1.

Table 1: Summary of Property Changes in Ti-64 Before and After HIP

Specimen	E (msi)	σ_y (ksi)	σ_{ult} (ksi)	Elong(%)
Before HIP				
BRT1ZA	16.24	163.7	185.9	8.14
BRT2ZA	16.52	166	185.9	8.36
BRT3ZA	16.11	166.0	187.1	11.73
FLT1ZA	16.25	163.6	184.7	6.77
FLT2ZA	16.40	165.2	186.2	8.08
FLT3ZA	15.77	164.2	185.4	7.04

Specimen	E (msi)	σ_y (ksi)	σ_{ult} (ksi)	Elong(%)
Average Before HIP	16.21 ± .26	164.78 ± 1.1	185.87 ± .80	8.35 ± 1.78
After HIP				
BRT4ZA	17.38	135.2	149.7	16.24
BRT5ZA	17.18	135.3	150.1	17.17
FLT4ZA	17.14	136.4	150.5	12.65
FLT5ZA	17.58	136.0	150.6	15.07
Average After HIP	17.32 ± .20	135.73 ± .57	150.6 ± .41	15.28 ± 1.95

The effect of HIP processing AM Ti-5553 is summarized in Figure 7. In Ti-5553, the HIP processing had a similar effect on ductility in that the elongation increased slightly, which is probably due to the decrease in number and size of defects that result from the AM process. The pressure and temperature of HIP should reduce the size and density of defects in the material. However, the yield strength increased after HIP in Ti-5553, which is the opposite behavior of what was observed in Ti-64. This is probably the result of a change in the phase content of the alloy as a result of heat treatment during HIP.

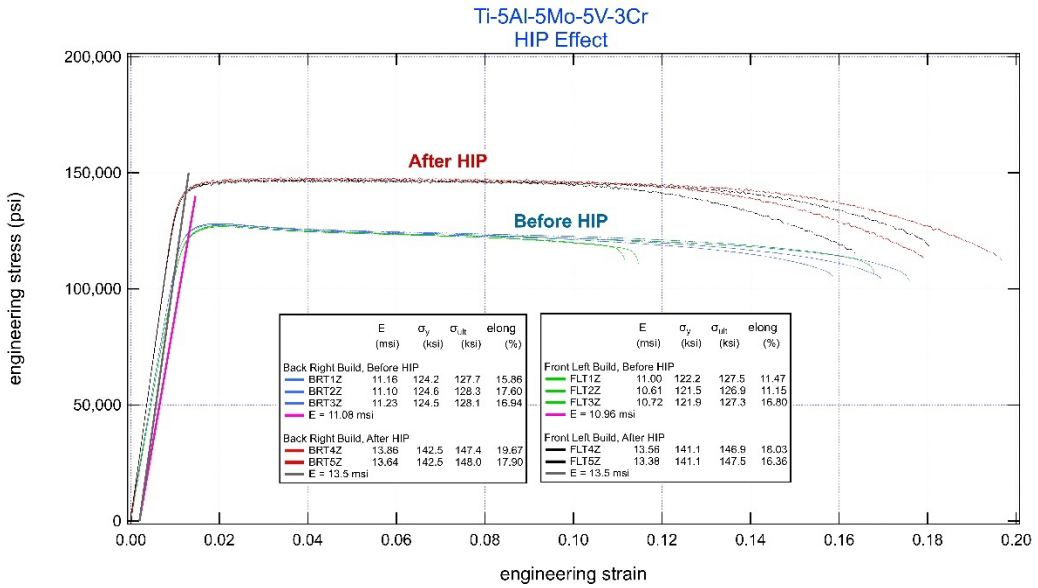

Figure 7: Effect of HIP processing on AM Ti-5553.

The property changes for Ti-5553 are summarized in Table 1.

Table 2: Summary of Property Changes for Ti-5553 before and after HIP Processing.

Specimen	E (msi)	σ_y (ksi)	σ_{ult} (ksi)	Elong(%)
Before HIP				
BRT1ZA	11.16	124.2	127.7	15.86

Specimen	E (msi)	σ_y (ksi)	σ_{ult} (ksi)	Elong(%)
BRT2ZA	11.10	124.6	128.3	17.60
BRT3ZA	11.23	124.5	128.1	16.94
FLT1ZA	11.0	122.2	127.5	11.47
FLT2ZA	10.61	121.5	126.9	11.15
FLT3ZA	10.72	121.9	127.3	16.80
Average Before HIP	10.97 $\pm$ .25	123.15 $\pm$ 1.42	127.633 $\pm$ .52	14.97 $\pm$ 2.89
After HIP				
BRT4ZA	13.86	142.5	147.4	19.67
BRT5ZA	13.64	142.5	148	17.90
FLT4ZA	13.56	141.1	146.9	18.03
FLT5ZA	13.58	141.1	147.5	16.36
Average After HIP	13.66$\pm$ .14	141.8 $\pm$ .81	147.45 $\pm$ .45	17.99 $\pm$ 1.35

The resultant properties after HIP processing were quite different for the two alloys. This is most easily summarized in Figure 8 below. While Ti-64 experienced a decrease in yield strength and an increase in ductility, the yield strength of Ti-5553 increased with only a small increase in ductility. Also, the standard deviation of the Ti-5553 ductility decreased after HIP. One important result is that the properties of both alloys become very similar (almost identical) after the same HIP treatment is applied to the as-built condition.

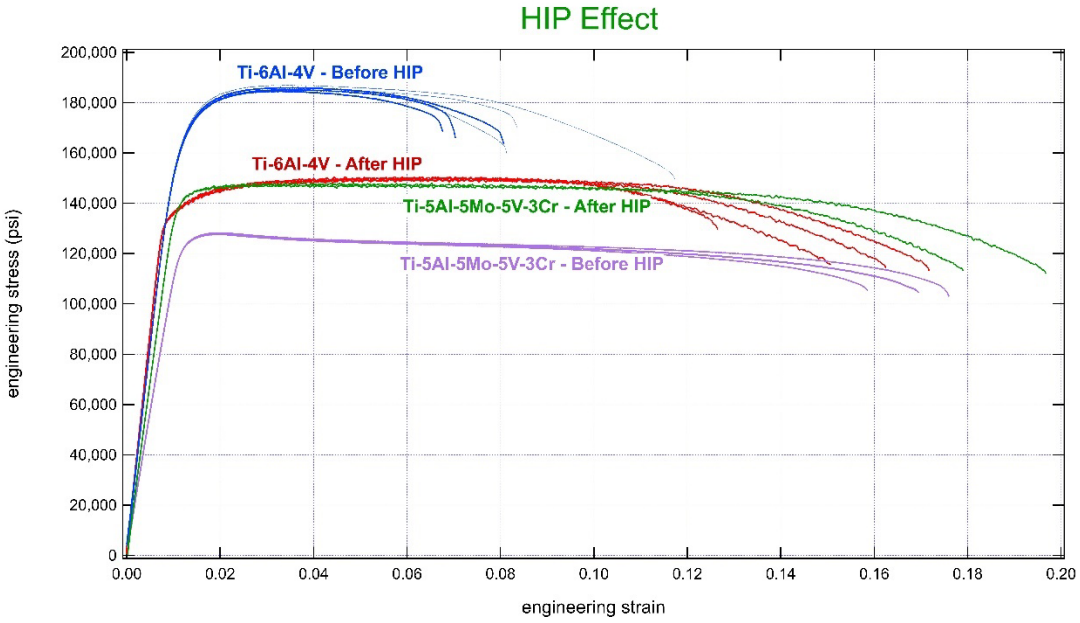

Figure 8: Comparison of HIP Processing Effects on Both AM Ti-64 and AM Ti-5553.

Table 3: Comparison of Averaged Properties of Ti-64 and Ti-5553 Before and After HIP.

	E (msi)	σ_y (ksi)	σ_{ult} (ksi)	Elong(%)		E (msi)	σ_y (ksi)	σ_{ult} (ksi)	Elong(%)
Ti-64 Before HIP	16.21 ± .26	164.78 ± 1.1	185.87 ± .80	8.35 ± 1.78	**Ti-5553** Before HIP	10.97 ± .25	123.15 ± 1.42	127.633 ± .52	14.97 ± 2.89
Ti-64 After HIP	17.32 ± .20	135.73 ± .57	150.6 ± .41	15.28 ± 1.95	**Ti-5553** After HIP	13.66± .14	141.8 ± .81	147.45 ± .45	17.99 ± 1.35

In the next section, the microstructural evolution of the alloys before and after HIP will be investigated to explain the mechanical property differences that are observed.

3.2. Microstructural Evolution Before and After HIP

3.2.1. Microstructural Evolution in Ti-64

Given the changes in mechanical properties observed in Figure 8, the microstructural evolution of Ti-64 and Ti-5553 is expected to be quite different. First, the as-received condition of Ti-64 will be shown. During the AM PBF process, the Ti-64 powder is rapidly solidified from the melt. The resultant microstructure is almost completely in the α phase. Figure 9 below shows the microstructure measured with EBSD of as-received Ti-64. Two different as-received samples are measured, and (a) and (d) show the phase content of the two regions. The regions are almost completely in the α phase, with less than 1% of the β phase retained at room temperature.

The orientation of the α lathes is visible in Figure 9 (b) and (e). There is no obvious preference for orientation according to the maps. The structure of the α phase is quite complex. However, it is possible to calculate what the parent β-phase grain structure looked like at elevated temperature based on the known orientation relationships between α and β Ti. These parent β-phase structures are shown in Figure 9 (c) and (f). These images allow a visualization of the grain structure at elevated temperature before the transformation to the α phase happens upon cooling.

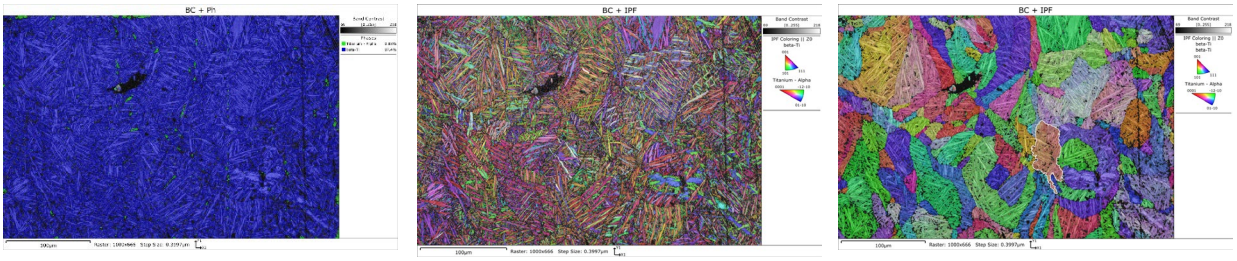

(a) (b) (c)

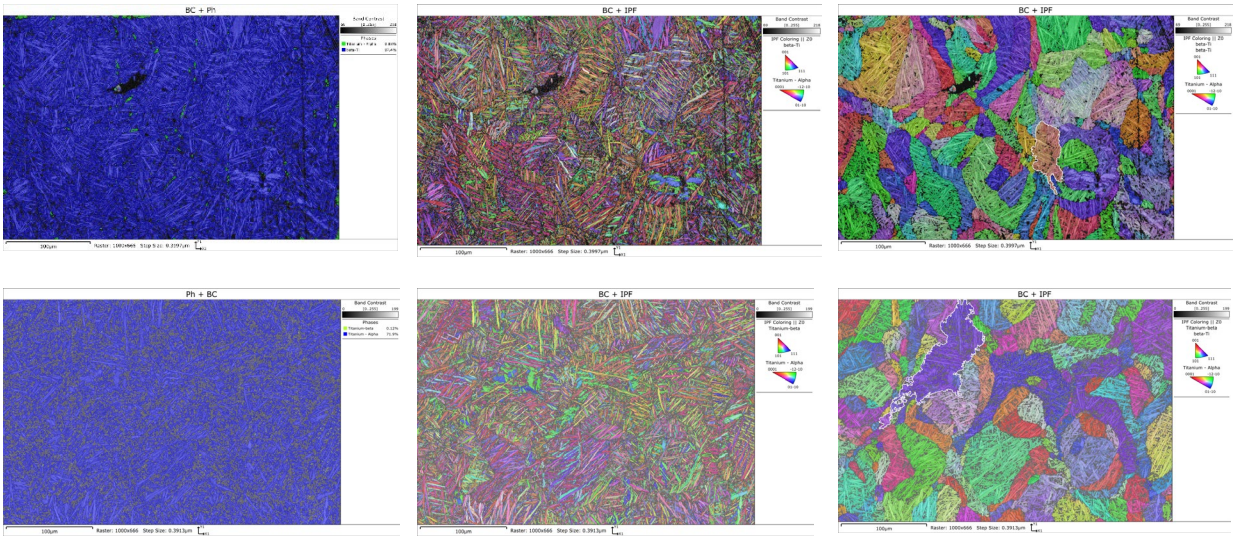

(d) (e) (f)

Figure 9: EBSD phase maps (a) and (d), IPFZ maps (b) and (e), and parent grain maps (c) and (f) for as-built Ti-64.

In both regions, the grain size is measured from the EBSD data. The α lathes have a measured ECD of approximately 4 μm, but the parent β grain size is ten times larger and approximately 40 μm ECD. There is no orientation preference or texture found in these samples. A typical pole figure is shown in Figure 10 and shows a mostly random distribution of grain orientation.

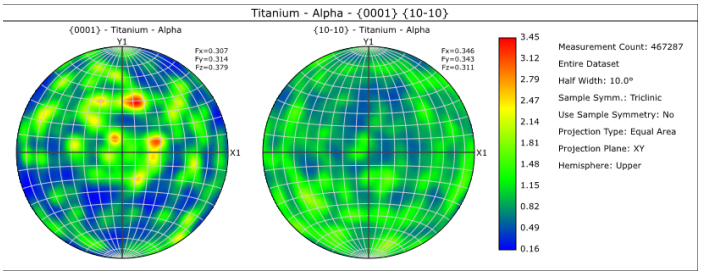

Figure 10: Pole Figure for as-built Ti-64.

The composition of the as-built Ti-64 is uniform at the scale of SEM-EDS measurements. The measured composition is approximately equivalent to the expected Ti-6 wt. % Al- 4 wt. % V composition. There is a region near the surface that appears to be slightly enriched in O. This "skin" region near the surface is approximately 2 μm, which is not expected to make changes to the bulk mechanical behavior. Measured composition maps and a quantitative line profile are shown in Figure 11. The high O content (~90 wt.%) near the top of the image is from the mounting epoxy resin.

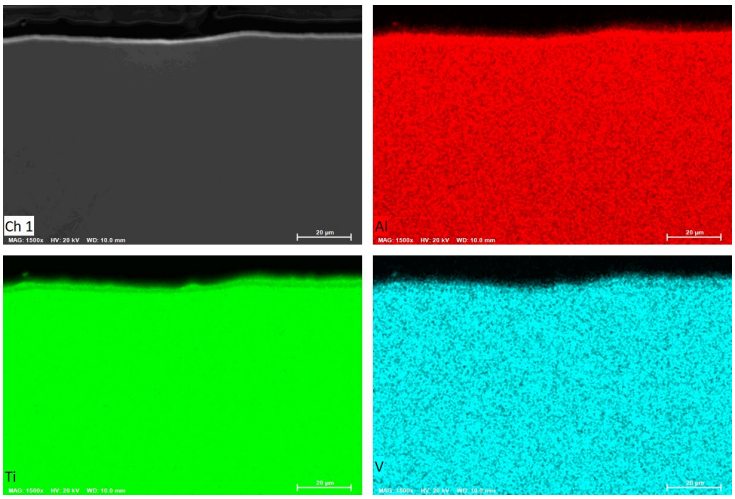

(a)

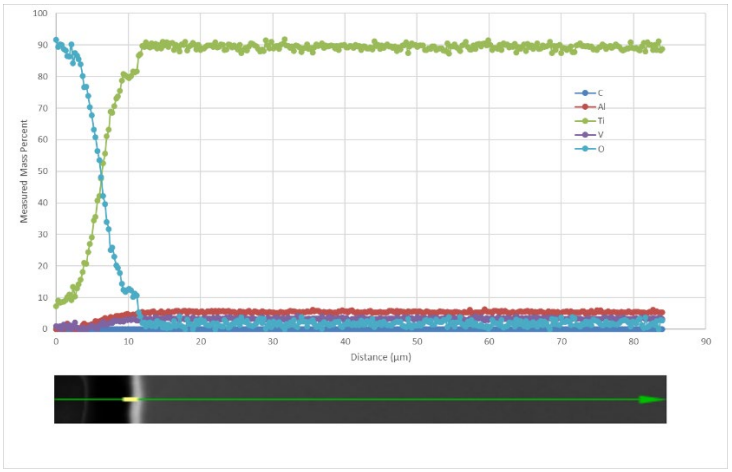

(b)

Figure 11: EDS composition maps (a) and standardless quantification of a line profile from the surface into the bulk (b). The composition is uniform, and there is evidence of a 1-2 µm thick oxide skin near the surface.

After HIP, the Ti-64 microstructure is not obviously different than the as-built condition. The EBSD measures still mostly α phase as shown in Figure 12. There is a small amount of retained β that is seen, but it still only comprised about 1% of the areas measured. The α lathes seem to have coarsened a small amount with the average size increasing from 4 µm before HIP to ~6.5 µm after HIP. The biggest difference observed in the EBSD maps is the increase in grain size of the parent β grains. After HIP, the parent grain size ECD increases to 50-60 µm, compared to 40 µm before HIP. Some of the softening behavior in the alloy could potentially be explained by the slightly larger parent grain size, but the observed change is not that large. There should be another strengthening mechanism with a larger change after HIP that can explaining the decrease in yield strength of Ti-64 after HIP.

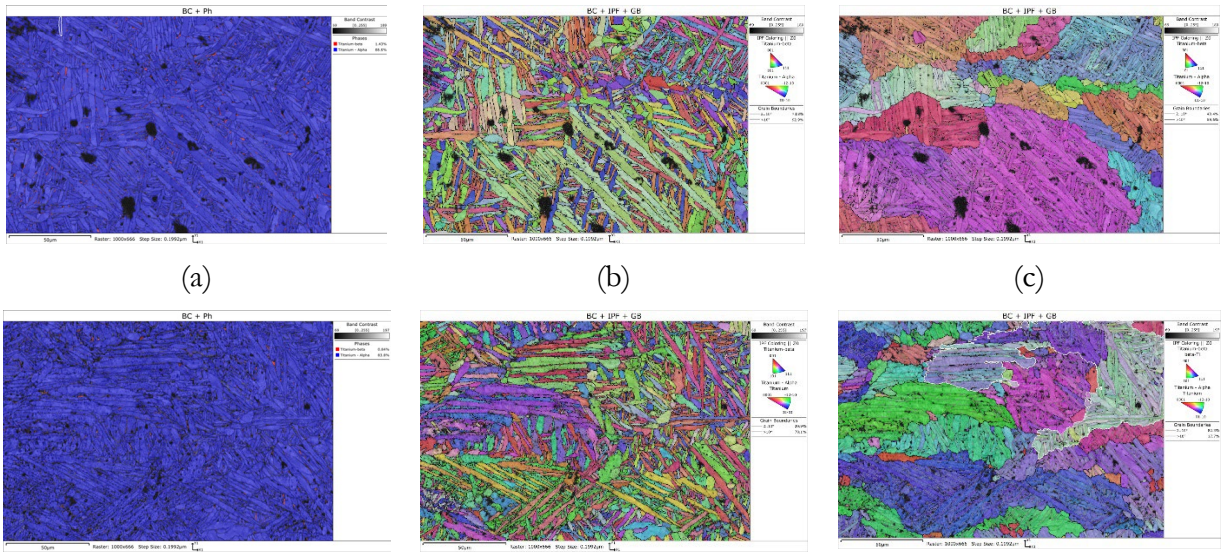

Figure 12: EBSD phase (a) and (d), IPFZ (b) and (e), and parent grain IPFZ (c) and (f) maps for HIP Ti-64.

In order to further evaluate how the HIP processing of Ti-64 could result in a decrease in the yield strength, GND was evaluated from the EBSD data. GND is an accepted way to measure dislocation substructure in materials, but it only measures those dislocations that are geometrically necessary, not all statistically significant dislocations [7-12]. Measurement of GND using EBSD-based techniques is not orientation dependent and works equivalently on single crystal and polycrystalline materials. Typically, adding dislocations to a material is a strengthening mechanism, so tracking the GND content in Ti-64 before and after the HIP process could reveal a reason behind the decrease in yield strength.

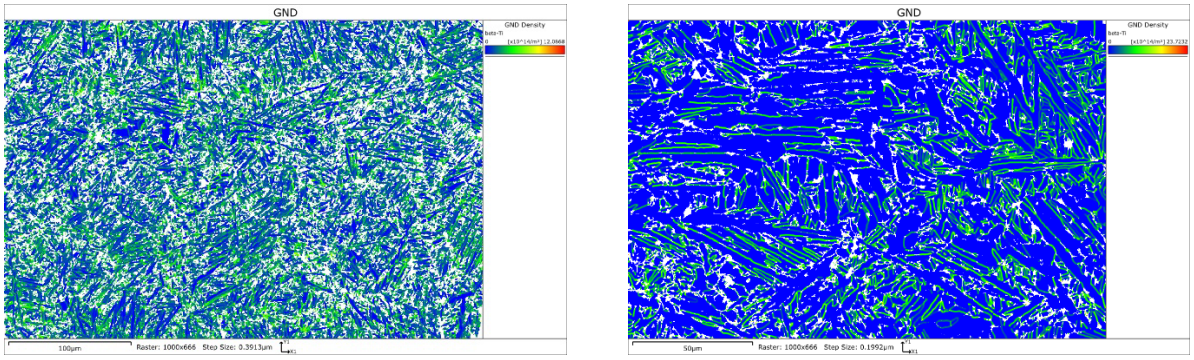

(a) (b)

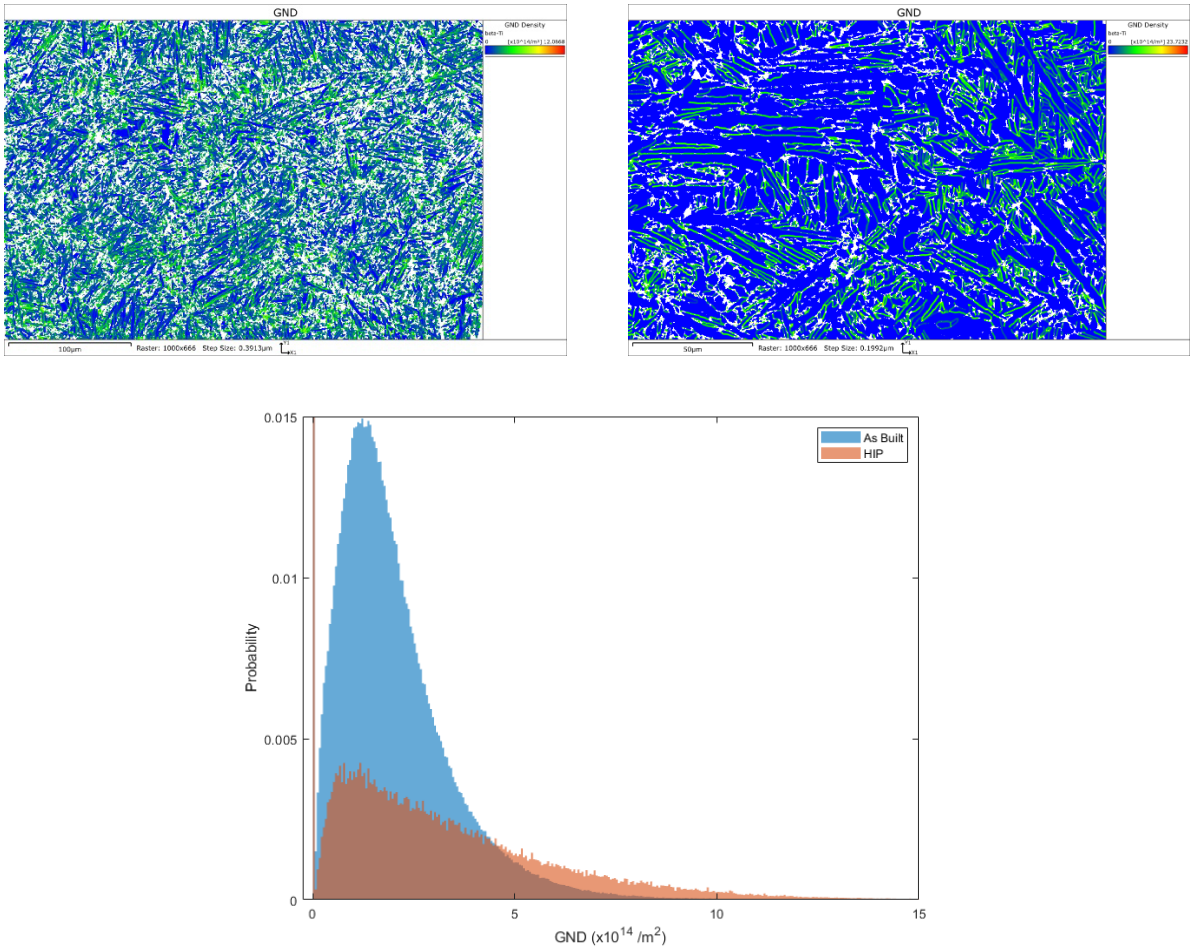

(c)

Figure 13: GND maps of (a) as-built Ti-64, (b), HIP Ti-64, and histogram plot comparing the GND distribution is shown in (c).

Maps showing the GND distribution in regions of as-built and HIP Ti-64 are shown in Figure 13 (a) and (b). Qualitatively, it is clear that the as-built condition has regions with relatively high dislocation content by the increased number of "greenish" pixels. In the HIP condition, there are many regions with blue pixels, which indicates low dislocation content, and then some small regions mostly near α-α boundaries that have increased dislocation content. It is possible to be more quantitative with a comparison between the two conditions by looking at a histogram of the dislocation density distribution in each map. This is shown in Figure 13 (c). In the as-built condition, there is a single peak in the GND distribution at 2-3x10^{14} /m^2. In the HIP condition, the peak is much less intense and shifted to lower dislocation density. In addition, the HIP condition has a huge peak at 0 /m^2, which would represent a completely recrystallized condition. Overall, the HIP condition does have regions with higher dislocation density than the as-built condition, as shown by the extension of the histogram to higher densities, but because the HIP condition also has a large peak at 0, the average dislocation content ends up being slightly lower in the HIP condition. Because the vast majority of the pixels have a lower dislocation content in the HIP condition, and because there are so many regions with no dislocations, it makes sense that a lower yield strength is measured in the HIP condition. The time, temperature, and pressure conditions of the HIP have enabled dislocation

climb and recrystallization such that the overall dislocation density goes down in most places, and small defects have healed out, which has increased the overall ductility of the Ti-64.

In addition to the GND changes, there are some interesting compositional changes that occur in Ti-64 as a result of HIP. In the as-built condition, the composition is mostly uniform at the scale of SEM with perhaps a thin oxide rich skin at the surface (Figure 11). After HIP, there is some more clear compositional segregation to the surface as well as some V segregation to what appears to be α-α boundaries. Figure 14 (a) – (c) shows compositional maps and an extracted profile of the near surface region of HIP Ti-64. The maps show some slight Ti-enrichment and Al depletion in the surface region approximately 10 μm thick. In the bulk of the sample, as shown in Figure 14 (d) – (f), there are regions about 2 μm wide that are enriched in V and depleted in Ti and Al. The HIP process definitely does cause some compositional rearrangement in Ti-64 consistent with extended anneals in the two phase region of the phase diagram. The fact that the temperature is high enough during HIP to cause atomic rearrangements like those shown in Figure 14 is further evidence that there is enough atomic rearrangement to eliminate dislocation density as discussed in Figure 13 above.

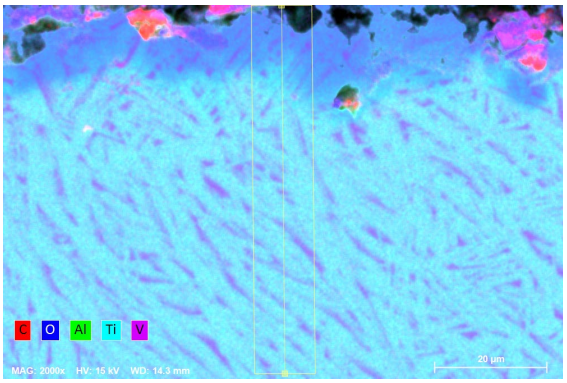

(a)

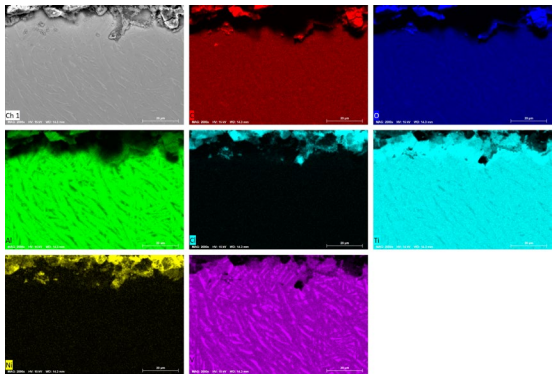

(b)

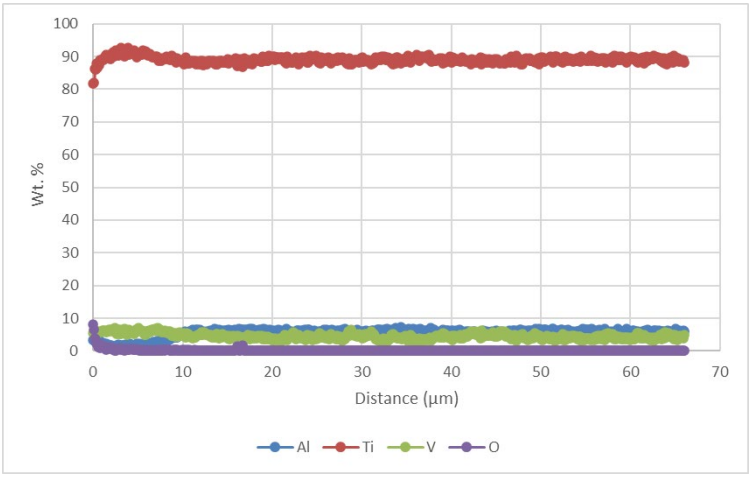

(c)

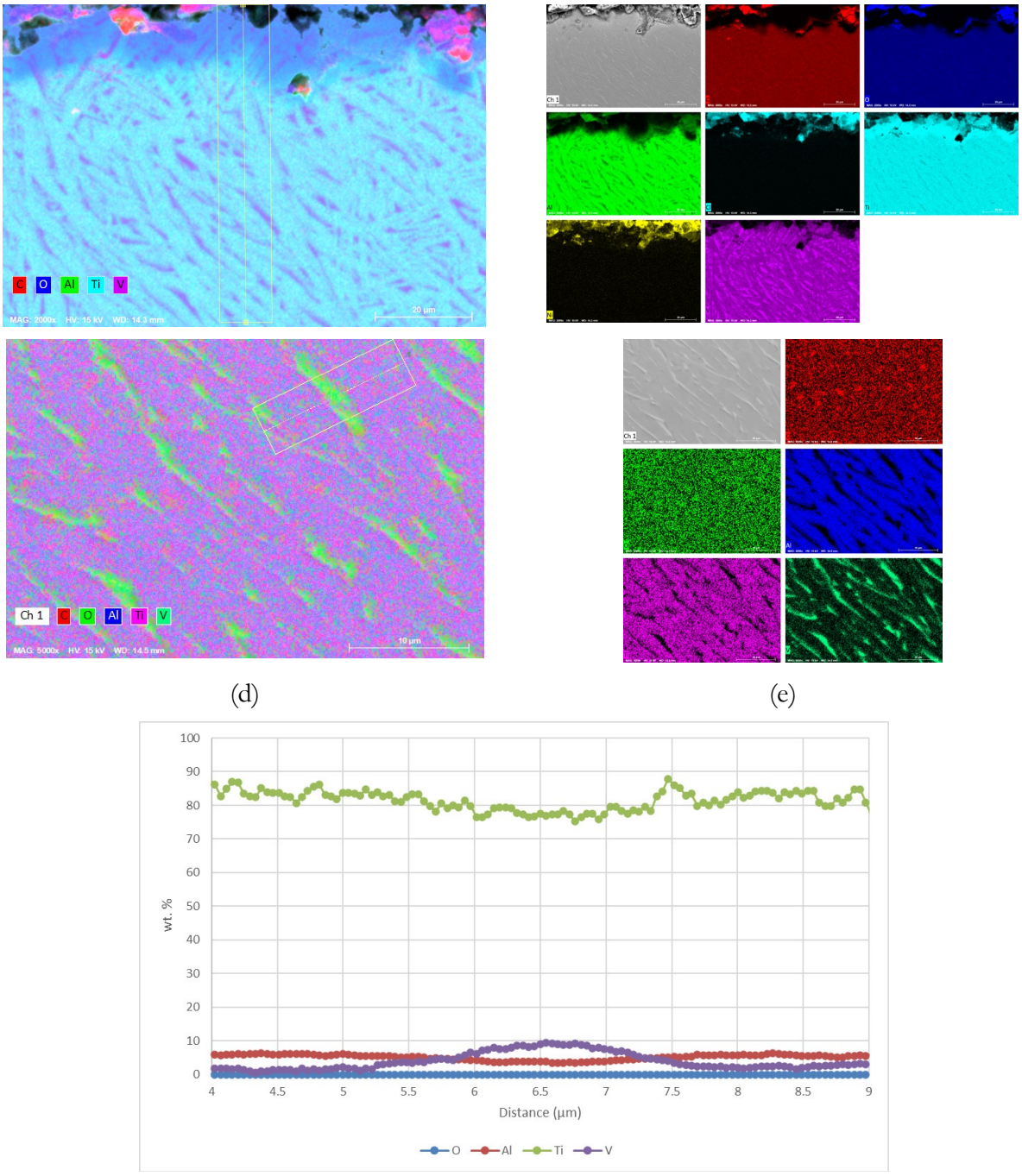

Figure 14: EDS maps and composition profiles for Ti-64 in the HIP condition. Lower magnification maps that show the enrichment of Ti and depletion of Al at the surface are shown in (a) – (c). A higher magnification map that shows V segregation to the α-α boundaries is shown in (d) – (f).

Finally, after HIP, there is no evidence of a preferred texture forming in Ti-64. The pole figure is fairly random and does not suggest any texture or orientation preference as a result of HIP. The pole figure is shown in Figure 15.

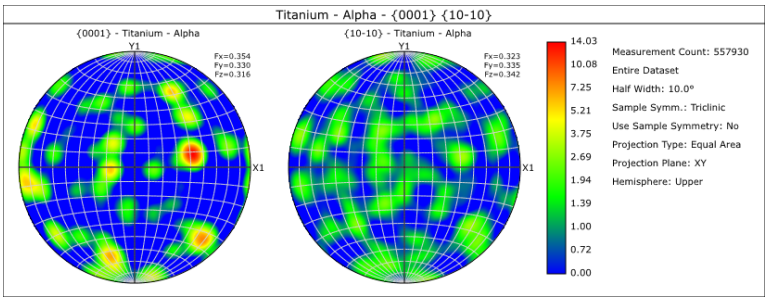

Figure 15: Pole Figure for HIP Ti-64 showing no particular texture or orientation preference as a result of HIP processing.

3.2.2. Microstructural Evolution in Ti-5553

Ti-5553 is a β-stabilized alloy, so in the as-built condition the microstructure is quite different than Ti-64 in that it is completely in the bcc β phase. The EBSD data for as-built Ti-5553 confirms that it is completely in the β phase. EBSD maps that show phase, IPFZ, and GND distribution are shown in Figure 16.

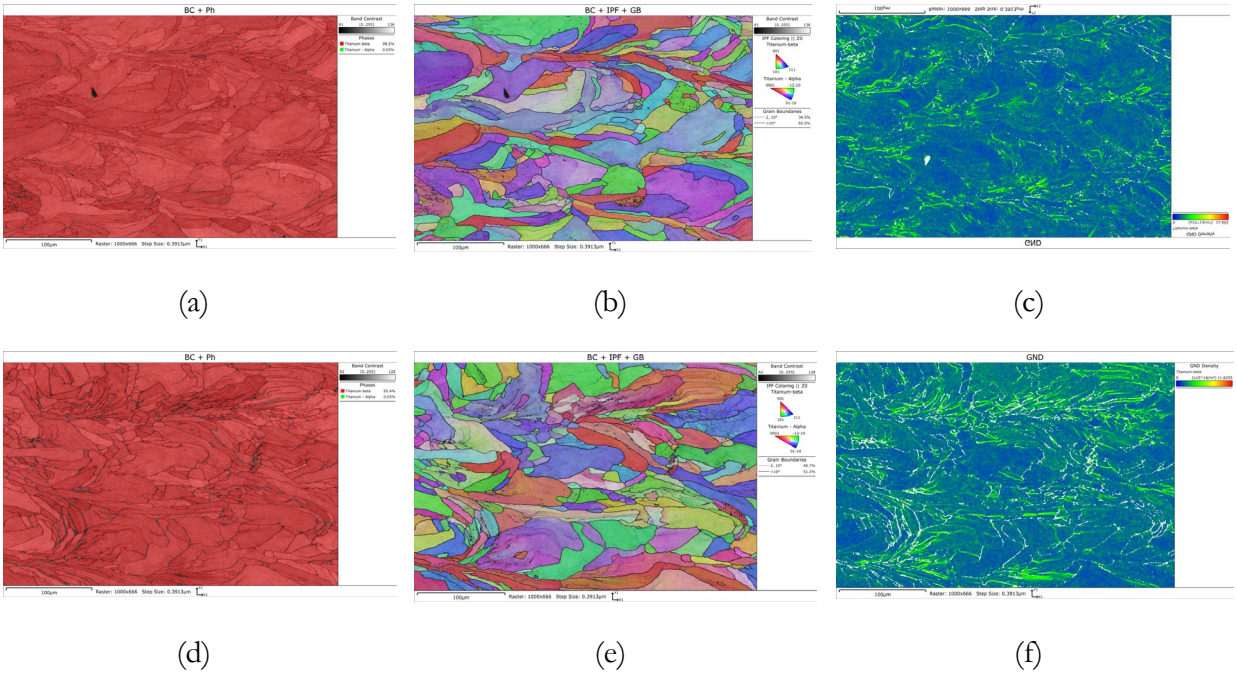

Figure 16: Phase maps (a) and (d), IPFZ maps (b) and (e), and GND maps (e) and (f) measured from EBSD in as-built Ti-5553.

After HIP, there is a noticeable change in the phase content of Ti-5553. As shown in Figure 17, the Ti-5553 has undergone a transformation that results in approximately 20% α-phase being present in the microstructure. The α phase is found both at the β-β grain boundaries, but it is also found in the interiors of the grains. This fine distribution if α phase is a likely candidate for the strengthening of Ti-5553. The large area of α/β interfaces creates an impediment to dislocation motion, and results in a strengthening of the Ti-5553 that is observed in Figure 7.

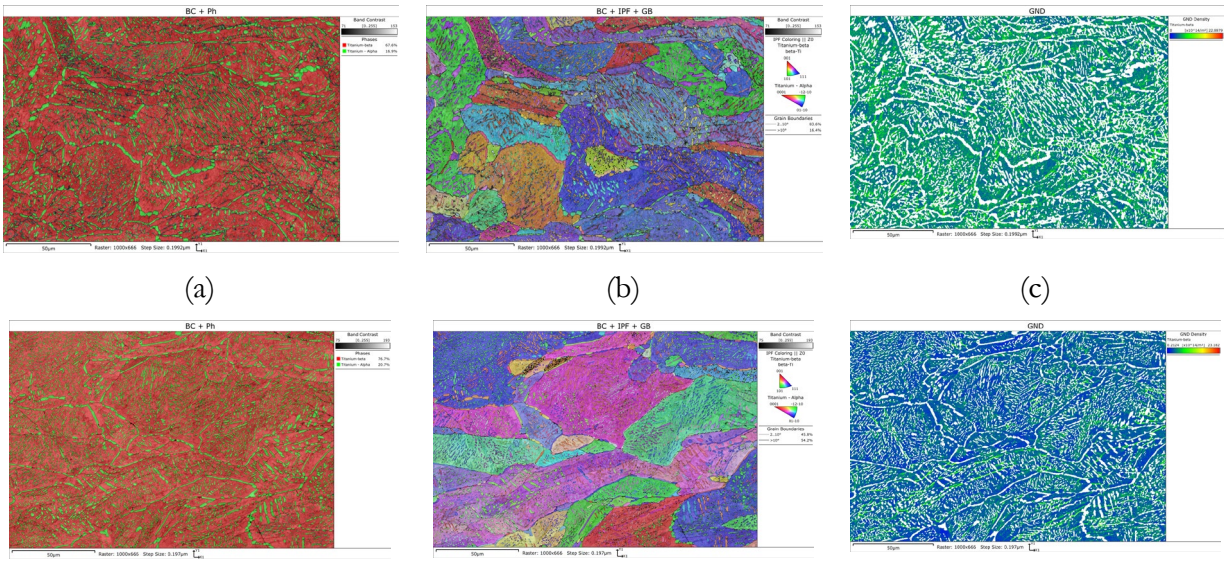

Figure 17: Phase maps (a) and (d), IPFZ maps (b) and (e), and GND maps (e) and (f) measured from EBSD in HIP Ti-5553.

In addition, the GND histograms can be compared before and after HIP. The GND distribution in the HIP material is shifted to higher dislocation densities. This suggests that the formation of α precipitates in the Ti-5553 as a result of the HIP process also results in some strain that induces the formation of dislocations in the microstructure. This could be due to the volumetric expansion that occurs during the β→α+β transformation [13]. The formation of these phase transformation induced dislocations also provides a strengthening mechanism for the Ti-5553. The GND histograms for Ti-5553 before and after HIP are shown in .

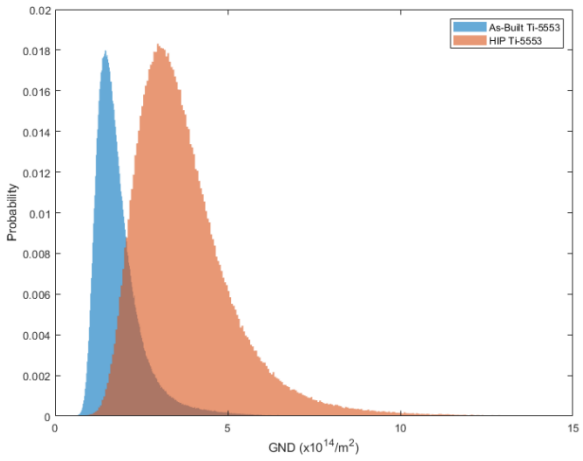

Figure 18: GND histogram plot comparing the GND distribution in as-printed and HIP Ti-5553. The data is taken from GND maps in Figure 16 (c) and (f) and Figure 17 (c) and (f).

As in Ti-64, there is no observed preferred texture or orientation in as-built or HIP Ti-5553. The EBSD-measured pole figures confirm this in Figure 19.

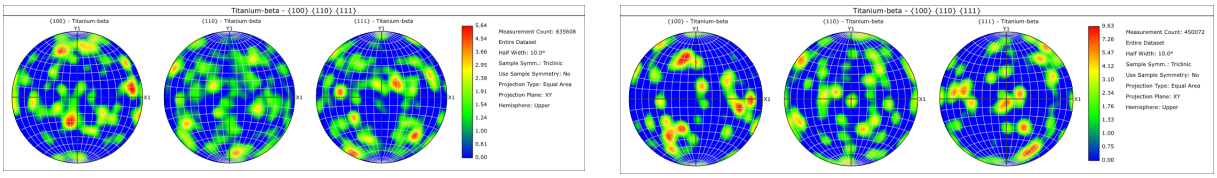

(a) (b)

Figure 19: Pole figure for as-built Ti-5553 (a) and HIP Ti-5553 (b) showing no orientation preference or texture.

As a result of the HIP process, there are also compositional changes that occur in Ti-5553. Initially, the composition of the as-built Ti-5553 is relatively uniform, and there are no heterogeneities at the scale of the SEM. Composition maps and profiles measured with EDS are shown in Figure 20. An oxide skin at the surface is measured that is approximately 2 μm thick. The O-rich region is at the interface between an O-rich epoxy resin and the metal surface, so the absolute numbers from the standardless EDS quant should not be interpreted as the true composition of the surface there.

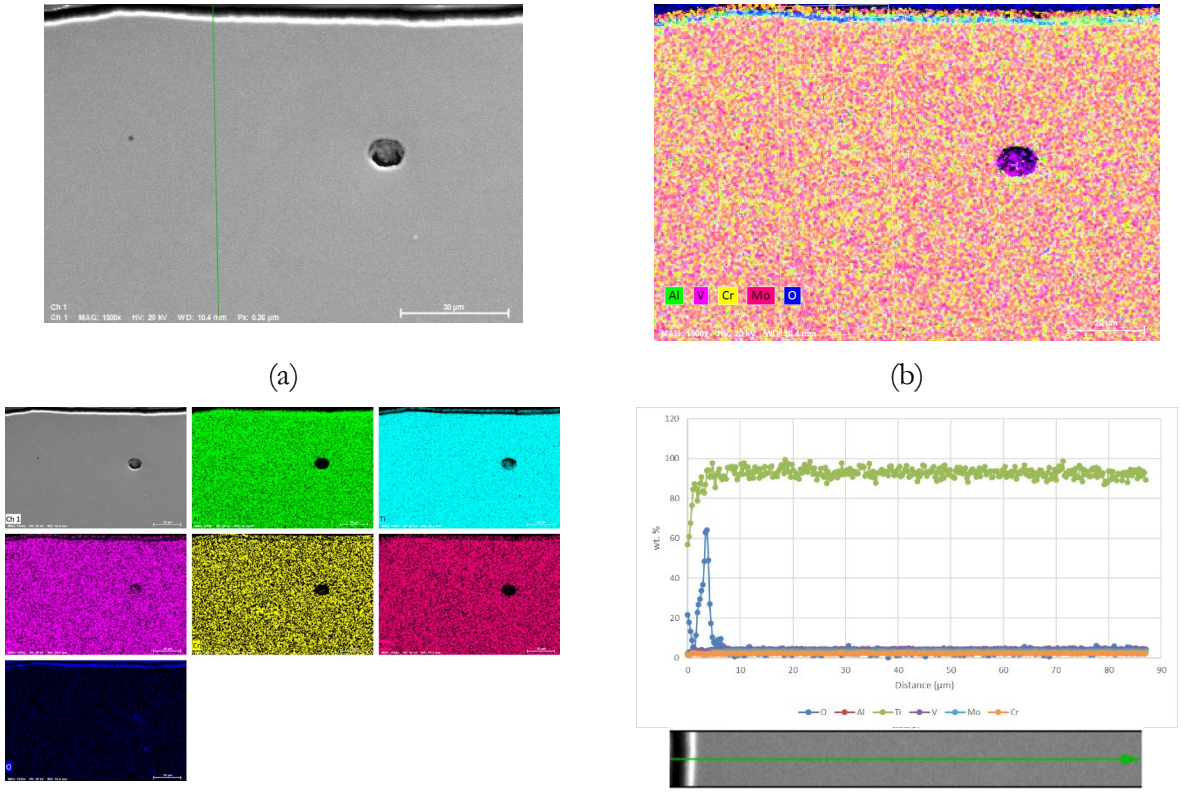

(a) (b)

(c) (d)

Figure 20: (a) SE image and (b) EDS composite map showing elemental distribution. Individual elemental maps are shown in (c), and a standardless quantification line profile is shown in (d) for as-printed Ti-5553.

After HIP, there are additional compositional changes that occur in Ti-5553 consistent with annealing in the two-phase region of the phase diagram. One change is to the composition in the near surface region as shown in Figure 21. Ti appears to have segregated to the near surface region and then slightly depleted Al. The changes are quite small and noisy and not they are not very

obvious. However, it is more obvious that the α regions are now enriched in Ti and Al and depleted in V, Mo, and Cr. It is interesting that in Ti-64, the α-α boundaries seem to enrich in Ti and V, in contrast to the α in Ti-5553, which is enriched in Ti and Al. Again, the HIP processing is at an elevated temperature where diffusion of atoms is active and compositional segregation occurs. It also suggests that the temperature is high enough for active diffusion and rearrangement of dislocation structures, which was also observed as explained in Figure 18 above. The activation energy for diffusion is likely effected by the residual strains that exist in the material as a result of the deposition process. The fact that we observe both changes in dislocation structure and composition as a result of the HIP process suggests that indeed, the temperature of the HIP process was enough to activate diffusion in these Ti alloys.

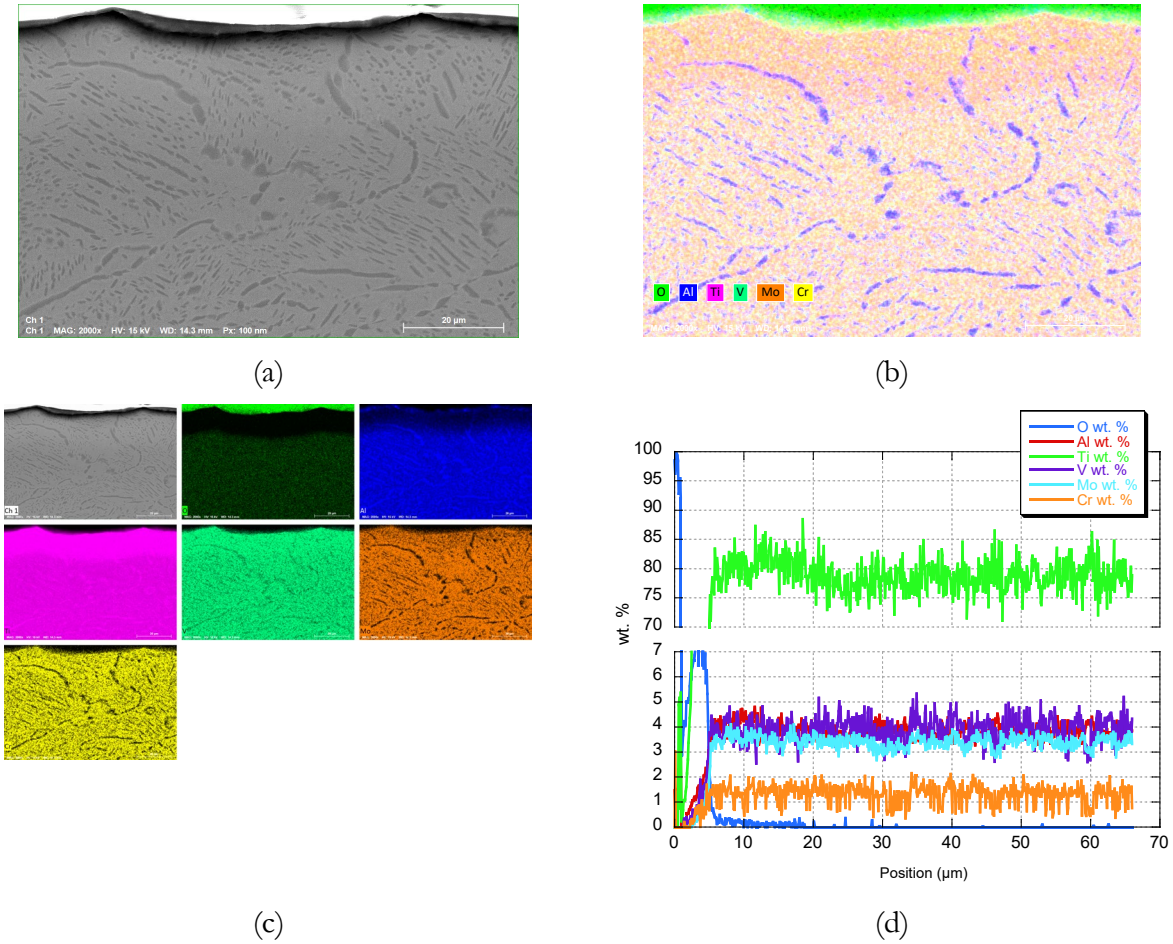

Figure 21: (a) SE image and (b) EDS composite map showing elemental distribution. Individual elemental maps are shown in (c), and a standardless quantification line profile is shown in (d) for HIP Ti-5553.

4. SUMMARY AND CONCLUSIONS

The effect of HIP on AM Ti-64 and Ti-5553 has been investigated. Both microstructural and mechanical property changes have been observed and documented.

- In Ti-64, there is decrease in the yield strength and increase in the ductility as a result of the HIP process.
    - The decrease in yield strength is due to the reorganization of dislocations into regions free of dislocations, and a small number of regions near α-α boundaries that are high in dislocation content.
    - The increase in ductility is due to the shrinking of defects that serve as crack nucleation sites during plastic deformation.
    - There is also compositional segregation in Ti-64 that results in an increase in V content at α-α boundaries.
- In Ti-5553, there is an increase in the yield strength and a slight increase in ductility accompanied by a decrease in the standard deviation of elongation at failure.
    - The decrease in the standard deviation of elongation at failure is a result of a decrease in the number of defects that can nucleate cracks from the HIP process
    - The increase in yield strength is caused by the formation of the α phase precipitates, which act as precipitation hardeners and also causes an increase in dislocation content upon formation as a result of the volumetric expansion that occurs when β→α+β. Both dislocations and α/β interfaces act as impediments to dislocation motion that increase the yield strength.
    - There is also a compositional segregation that occurs where the α phase that forms at grain boundaries and in grain interiors is enriched in Al.

REFERENCES

1. Yang, N., et al., *Metallurgy, Mechanical Property, AM Sidewall Roughness and Mitigation, and Manufacturing Limit for PBF-Ti64 Prototypes*. 2020, Sandia National Laboratories.
2. Beal, J.D., R. Boyer, and D. Sanders, *Forming of Titanium and Titanium Alloys*, in *Metalworking: Sheet Forming*. 2006, ASM International. p. 0.
3. Boyer, R.R., *Introduction and Overview of Titanium and Titanium Alloys*, in *Metals Handbook Desk Edition*. 1998, ASM International. p. 0.
4. Cotton, J.D., et al. *Phase Transformations in Ti-5Al-5Mo-5V-3Cr-0.5Fe*. in *11th, World conference on titanium; Ti-2007 science and technology; JIMIC5*. 2007. Sendai, Japan, Kyoto, Japan: Japan Institute of Metals;.
5. Boyer, R.R., *Processing of Titanium and Titanium Alloys*, in *Metals Handbook Desk Edition*. 1998, ASM International. p. 0.
6. Smith, T.R., et al., *Relationship between manufacturing defects and fatigue properties of additive manufactured austenitic stainless steel.* Materials Science and Engineering: A, 2019: p. 138268.
7. Kamaya, M., *Assessment of local deformation using EBSD: Quantification of accuracy of measurement and definition of local gradient.* Ultramicroscopy, 2011. **111**(8): p. 1189-1199.
8. Kubin, L.P. and A. Mortensen, *Geometrically necessary dislocations and strain-gradient plasticity: a few critical issues.* Scripta Materialia, 2003. **48**(2): p. 119-125.
9. Moussa, C., et al., *About quantitative EBSD analysis of deformation and recovery substructures in pure Tantalum.* IOP Conference Series: Materials Science and Engineering, 2015. **89**: p. 012038.
10. Moussa, C., et al., *Statistical analysis of dislocations and dislocation boundaries from EBSD data.* Ultramicroscopy, 2017. **179**: p. 63-72.
11. Pantleon, W., *Resolving the geometrically necessary dislocation content by conventional electron backscattering diffraction.* Scripta Materialia, 2008. **58**(11): p. 994-997.
12. Wilkinson, A.J. and D. Randman, *Determination of elastic strain fields and geometrically necessary dislocation distributions near nanoindents using electron back scatter diffraction.* Philosophical Magazine, 2010. **90**(9): p. 1159-1177.
13. lshaer, R., Ibrahim, K. , Barakat, A. , Farahat, A. and Abbas, R., *Determination of Phase Transformation for TC21 Ti-Alloy by Dilatometry Method.* Open Journal of Metal, 2019. **9**: p. 1-10.

DISTRIBUTION

Email—Internal

Name	Org.	Sandia Email Address
Technical Library	1911	sanddocs@sandia.gov

Email—External

Name	Company Email Address	Company Name

Hardcopy—Internal

Number of Copies	Name	Org.	Mailstop

Hardcopy—External

Number of Copies	Name	Company Name and Company Mailing Address

This page left blank

Sandia National Laboratories

Sandia National Laboratories is a multimission laboratory managed and operated by National Technology & Engineering Solutions of Sandia LLC, a wholly owned subsidiary of Honeywell International Inc. for the U.S. Department of Energy's National Nuclear Security Administration under contract DE-NA0003525.